ELSEVIER

Contents lists available at ScienceDirect

Computers and Geotechnics

journal homepage: www.elsevier.com/locate/compgeo



Solid-like to liquid-like transition of stick-slips in sheared fault gouge

Yahui Zhang ^a, Zifan Li ^a, Ke Gao ^{b,*}, Huiming Tang ^{a,c}, Changdong Li ^{a,c}, Zerui Wang ^a

- ^a Faculty of Engineering, China University of Geosciences, Wuhan 430074, Hubei, China
- b Department of Earth and Space Sciences, Southern University of Science and Technology, Shenzhen 518055 Guangdong, China
- ^c Badong National Observation and Research Station of Geohazards, China University of Geosciences, Wuhan 430074, China

ARTICLE INFO

Keywords:
Stick-slip
Fault gouge
Particle kinematics
Solid-like to liquid-like state transition

ABSTRACT

The macroscopic stick–slip motion observed in sheared fault gouges fundamentally emerges from the microscopic interactions among constituent particles. In this work, we numerically investigate the universality of stick–slip dynamics in a fault gouge by analyzing particle-level kinematics, where particle assembly is traced in terms of their positions and velocities. Specifically, we disentangle the contributions of velocity magnitude and direction to the overall dynamics. In the stick regime, the gouge system exhibits strong spatial correlations, manifested by the coherent particle motion regarding both velocity magnitude and direction, as well as long-range velocity correlations across the entire system. In contrast, the slip phase is triggered by the breakdown of these long-range correlations, driven by localized high-speed motion and directional disorganization. Notably, high-speed regions emerge where particles move opposite to the shearing direction, resembling turbulent eddies in fluid flow. These observations provide a phenomenological framework for interpreting stick–slip transition as a solid-like to liquid-like state transition. Our findings not only deepen the understanding of the fundamental physics underlying stick–slip transitions but also bear significant implications for practical applications in various fields, such as shear failure of sliding surfaces or sliding zones in landslides.

1. Introduction

Stick-slip motion represents a ubiquitous interfacial instability phenomenon observed across multiple scientific disciplines, from microscale physics (e.g. Gourdon and Israelachvili, 2003; Mulliah et al., 2004) to geological manifestations such as earthquake faults (e.g. Brace and Byerlee, 1966; Johnson et al., 2008) and landslides (e.g. Yamada et al., 2016; Finnegan et al., 2022). This dynamic process, characterized by interrupted motion between two sliding surfaces accompanied by sudden shear stress release, contrasts fundamentally with smooth, uninterrupted motions (Yoshizawa et al., 1993). Understanding the origin of stick-slip is crucial for a wide range of physical, geological and industrial applications, such as the jamming-unjamming transition in granular materials, rock avalanches, and the breakdown of bulk metallic glasses. Extensive laboratory friction experiments have demonstrated that even under a constant force or sliding velocity, a complex spectrum of stick-slip dynamics can emerge, up to differences stemming from the system parameters (the inertia, stiffness, and the friction of the interacting bodies, etc.) (e.g. Lieou et al., 2015; Pugnaloni et al., 2022) as well as experimental conditions like various relaxation times and previous history (e.g. Anthony and Marone, 2005). As a result, it is unrealistic to expect that findings from one system can be directly generalized to another (Berman et al., 1996), particularly for granular materials which exhibit rich bifurcation behaviors arbitrarily analogous to solids, fluids (e.g. Kou et al., 2017), gas, or intermediate phases (e.g. Kozlowski et al., 2022).

To predict and subsequently control undesirable stick–slip motion in natural systems, the dynamics of stick–slip have been investigated at the constituent structural level. Recent advancements in the physics of granular materials indicate that stick–slip dynamics manifests as a solid-like to liquid-like transition, triggered when the applied shear stress exceeds a critical threshold (Buldum and Ciraci, 1997; Lyashenko and Zaskoka, 2013). In this sense, stick and slip represent two distinct motion states emerging from the collective behavior of constituent particles (Hayman et al., 2011). However, a comprehensive understanding of stick–slip dynamics faces two significant challenges: first, the system must remain tractable for microscopic dynamics while simultaneously capturing the macroscopic behavior; second, a control mechanism must be devised to bridge individual particle behaviors with the overall mechanical performance of the system (Zheng et al., 2018). Particle-level

E-mail address: gaok@sustech.edu.cn (K. Gao).

 $^{^{\}ast}$ Corresponding author.

information has been experimentally investigated through the implementation of advanced synchronous observation techniques, including synchrotron x-ray imaging (e.g. Cao et al., 2018) and photoelasticimetry of force chains (e.g. Abed Zadeh et al., 2019; Shang et al., 2024). Despite these methodological advances, most experimental studies on stick—slip in granular materials are limited to hard-sphere systems (disks in two dimensions), such as glass beads and photoelastic particles. Notably, experimental determination of dynamic properties at the particle level remains unachievable for three-dimensional granular systems (Kou et al., 2017). Numerical characterization techniques have been explored in the context ranging from molecular dynamics simulations at the nanoscale (e.g. Luan and Robbins, 2004) to particle-based numerical methods at the millimeter scale (e.g. Zhang et al., 2023). Nevertheless, a thorough investigation of the kinematic characteristics in stick—slip motion remains an open area of research.

In response to the challenges encountered in experimental approaches, we perform a numerical simulation of shearing a flat fault gouge system, aiming to bridge the gaps between the particle-scale kinematics and stick—slip instability. This focus is motivated by two key considerations. First, the gouge-contained fault model represents a realistic scenario for earthquake faults, which are typically filled with crushed rock grains generated by prolonged fault grinding. Second, the granular nature of the fault gouge offers a broad facility to track the particle-scale or millimeter-scale details. In this study, we analyze the kinematics of the gouge system by examining particle motion in terms of both speed (defined as the magnitude of velocity) and direction.

Our findings provide a mechanistic framework for interpreting the stick—slip transition, defining the solid-like state not merely by low velocities but by high directional coherence and system-wide correlation. The subsequent transition to a liquid-like state is triggered by directional disorganization and the collapse of these spatial correlations. This physics-based criterion, which moves beyond mere kinematic description, offers a promising approach for identifying pre-failure signals in landslide slip zones, potentially paving the way for new early-warning strategies.

2. Methods

2.1. Numerical model setup

The two-dimensional numerical model is designed based on the laboratory photoelastic experiment reported by Geller et al. (2015). Details of the model calibration can be found in Gao et al. (2018). Fig. 1 shows the fault gouge sandwiched between two identical deformable plates with dimensions of 570 mm in width and 250 mm in height. The two plates are simulated using the finite element method (FEM) (Reddy, 2005), while the gouge layer is modeled employing the finite-discrete element method (FDEM) (Munjiza, 2004; Munjiza et al., 2006). To minimize model distortion, the upper and lower boundaries of the sheared system are constrained by two stiff bars. The whole fault gouge comprises 2,817 non-broken circular particles, with diameters of either 1.2 or 1.6 mm. To eliminate edge effects, only 1,917 particles located in the central region (see Fig. 1a) are considered in the analysis of particle kinematics. Additional material properties and simulation parameters are summarized in Table 1.

Table 1
Material and simulation parameters used in the numerical model.

Property	Value	Property	Value
Particle diameter	1.2 or 1.6 mm	Stiff bar density	2,800 kg/ m ³
Particle density	1,150 kg/ m ³	Stiff bar Young's modulus	30 GPa
Particle Young's modulus	0.4 GPa	Stiff bar Poisson's ratio	0.33
Particle Poisson's ratio	0.4	Foam density	1,150 kg/ m ³
Particle-particle friction coefficient	0.15	Foam Young's modulus	1 MPa
Number of particles	2,817	Foam Poisson's ratio	0.4
Main plate density	1,150 kg/ m ³	Contact penalty	4 GPa
Main plate Young's modulus	2.5 MPa	Time step	1.0E-7 s
Main plate Poisson's ratio	0.49	Normal load P	12-44 kPa
Particle–plate friction coefficient	0.15	Shear velocity V	0.5 mm/s

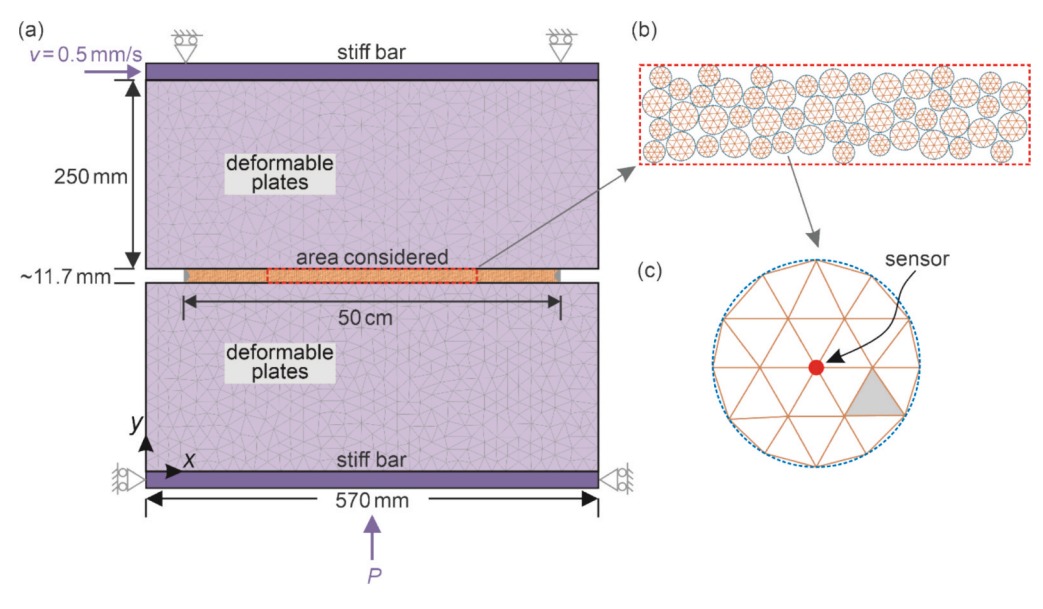


Fig. 1. (a) Schematic of the numerical model. The top and bottom plates are modeled as deformable structures using finite element meshes. (b) The fault gouge layer, represented by discrete particles randomly distributed and arranged in 9 rows and 313 columns between the plates prior to consolidation. The analyzed region comprises approximately 210 columns. (c) Meshed particles simulated using the finite-discrete element method (FDEM). Each particle is discretized into 24 approximately equal-sized triangle finite elements to capture its deformation, ensuring the particle shape approximates a circular geometry (indicated by dashed outlines). Particle velocities are derived from the displacements of sensors located at the geometric centers of the particles.

The model is conducted over a total duration of 27,000 ms under a constant normal load P=28 kPa and shear velocity V=0.5 mm/s. Throughout the simulation, the shear and normal forces acting between the particles and the upper and lower plates, as well as the particle positions, are recorded at 1 ms intervals, enabling the calculation of particle velocities. The ratio of the shear to normal force is calculated as the normalized shear stress between the plates and fault gouge. The system undergoes an initial consolidation phase, reaching a quasi-steady state after approximately 1/6 course of the run (\sim 5,000 ms). Therefore, data for analysis are extracted from 1,917 particles during the simulation time from 5,000 to 27,000 ms. The model design is in accordance with and thus can refer to our previous numerical study (Zhang et al., 2023).

2.2. Data processing of particle velocities

Particle kinematic measurements are initiated by tracking the sensor position of each particle (see Fig. 1c). The sensor positions are updated at intervals of 1 ms, generating raw data comprising x- and y-coordinates of the considered 1,917 particles over a simulation period spanning from 5,000 to 27,000 ms. The velocity of each particle, v_i , is calculated from its displacement vector $[\Delta x_i, \Delta y_i]$, where Δx represents the shear direction and Δy corresponds to the direction normal to the shear direction (as shown in Fig. 1a). In subsequent analyses, both the magnitude and direction of the particle velocity are examined independently to provide a comprehensive understanding of the kinematic behavior.

3. Results

3.1. Magnitude and direction of system velocity

Fig. 2a displays the simulation results, illustrating regular stick-slip

behavior at the steady state. To investigate the relationship between particle kinematics and stick–slip transition, four typical slip events (labeled as event A, event B, event C, and event D) are analyzed in detail. By taking the average over all particle speeds, the average speed, $\langle |\nu_i| \rangle$, is calculated to quantify the overall magnitude of particle velocities. The temporal evolution of theaverage speed is shown in Fig. 2b. Fig. 2c depicts the speed variance, which quantifies the spatial heterogeneity of particle speeds, calculated using the following formula:

$$|\nu|_{var} = \frac{1}{N} \sum_{i=1}^{N} (|\nu_i| - \langle |\nu_i| \rangle)^2$$
 (1)

where *N* is the total number of particles (N = 1,917 in this study), and $|v_i|$ is the speed of particle *i*. Throughout the paper, the notations $|\bullet|$ and $|\bullet|$ are used to denote the vector modulus and the average, respectively.

As observed from Fig. 2, the four typical slip events are evidently characterized by both elevated particle speeds (Fig. 2b) and significant speed variance (Fig. 2c). This observation can be logically interpreted as evidence of partial slip (Kozlowski et al., 2022), where localized regions with high particle speeds contribute to the overall increase in speed. Fig. 3 depicts the speed fields of the four sample events, alongside two stick phase for comparison. The results confirm the presence of small, localized areas that facilitate high-speed motion during fault slip (indicated by red to black regions in Fig. 3a-d). In contrast, during stick phases, particle speeds exhibit minimal variation, resulting in a rather homogeneous speed field (Figs. 3e and f).

To probe the directional alignment of particles independently of their speeds during the stick–slip transition, we introduce the polarized velocity as a metric to quantify the overall consistency in particle motion directions, defined as

$$\emptyset = \left| \left\langle \frac{v_i}{|v_i|} \right\rangle \right| \tag{2}$$

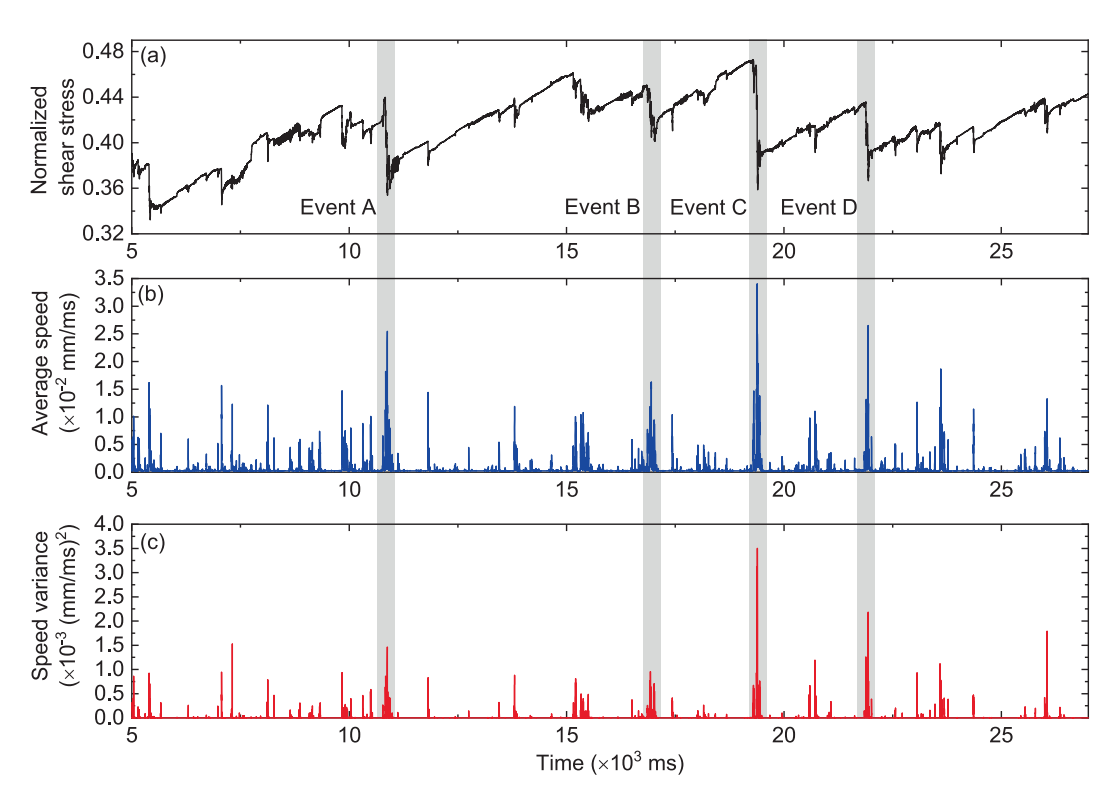


Fig. 2. (a) Temporal evolution of normalized shear stress (defined as the ratio of shear to normal stress between the plates and fault gouge) during the simulation. The shaded areas highlight the four typical slip events characterized by stress drops: event A (10.6 to 11.2×10^3 ms), event B (16.6–17.2 $\times 10^3$ ms), event C (19.2 to 19.6×10^3 ms), and event D (21.7 to 22.2×10^3 ms). (b) Temporal evolution of the average speed of the considered 1,917 gouge particles. (c) Temporal variation of the speed variance. Notably, the peak values of both average speed and speed variance coincide during the four slip events, which are denoted as $Speed_{max}^A = 10,877$ ms, $Speed_{max}^B = 16,950$ ms, $Speed_{max}^B = 19,384$ ms, and $Speed_{max}^D = 21,938$ ms.

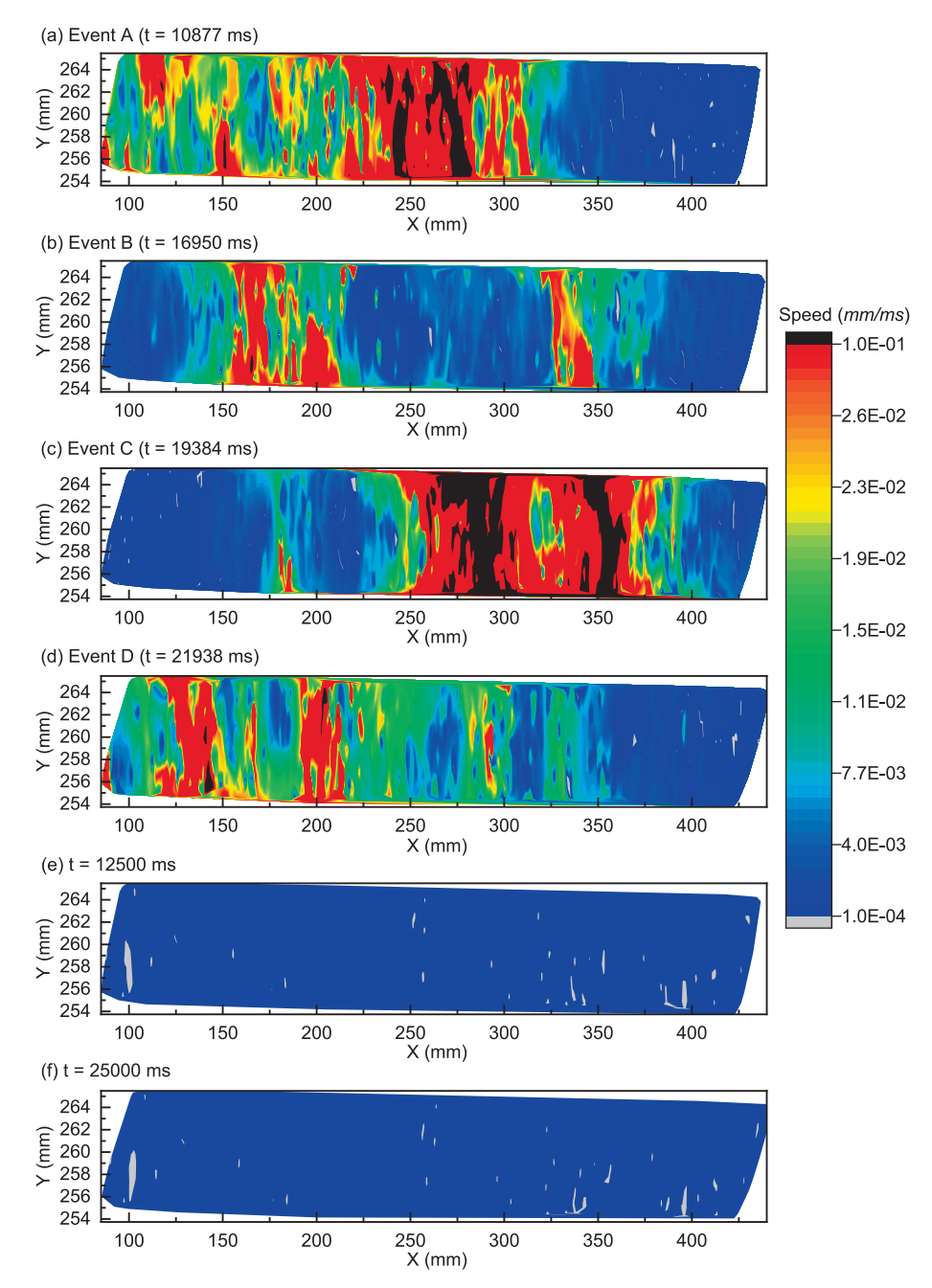


Fig. 3. Speed fields of the analyzed gouge particles at (a)-(d) the four sample slip events and (e)-(f) two stick phases. Note that the blank areas exist near the gouge boundaries due to the artifact of the natural neighbor interpolation method used.

The value Ø ranges from 0 to 1, with higher values indicating the system transitioning toward an ordered state due to consistent particle motion directions, and lower values suggesting a disordered state. Fig. 4 illustrates the temporal distribution of polarized velocity alongside normalized shear stress, revealing a close correlation between directional consistency (quantified by polarized velocity) and the two-state phase transition of stick–slip. During stick phases, the polarized velocity stabilizes around one, indicating that gouge particles move coherently in the same direction. In contrast, as slip proceeds, the polarized velocity drops sharply to zero, reflecting a loss of directional coherence as particles disperse in all directions. This behavior aligns with the conceptualization of stick–slip motion as a freezing-melting transition, where the system transites from a solid-like ordered state to a disordered or liquid-like state when the applied shear stress exceeds a critical threshold (Buldum and Ciraci, 1997; Lyashenko and Zaskoka, 2013).

To further analyze the distribution of particle velocity directions and magnitudes, Fig. 5 presents histograms of horizontal velocity, v(x), at the four sample slip events and two stick times considering either positive or negative direction. A comparison of the velocity profiles between slip (Fig. 55a-d) and stick (Fig. 55e-f) regimes reveals two distinctive characteristics. First, the magnitude of horizontal velocity during slip events is almost three orders higher than that of the stick regime. Second, the velocity profiles during stick phases exhibit a peak-like shape, indicating approximately uniform speed, which is consistent with the homogeneous speed fields observed in Fig. 3e-f. In contrast, slip events produce valley-like profiles, resulting from rapid particle motion in either the positive or the negative direction. Notably, a large number of particles exhibit high-speed motion in the negative direction during fault slips. This phenomenon can be attributed to high-speed particles (corresponding to black regions in Fig. 3a-d) reversing their direction

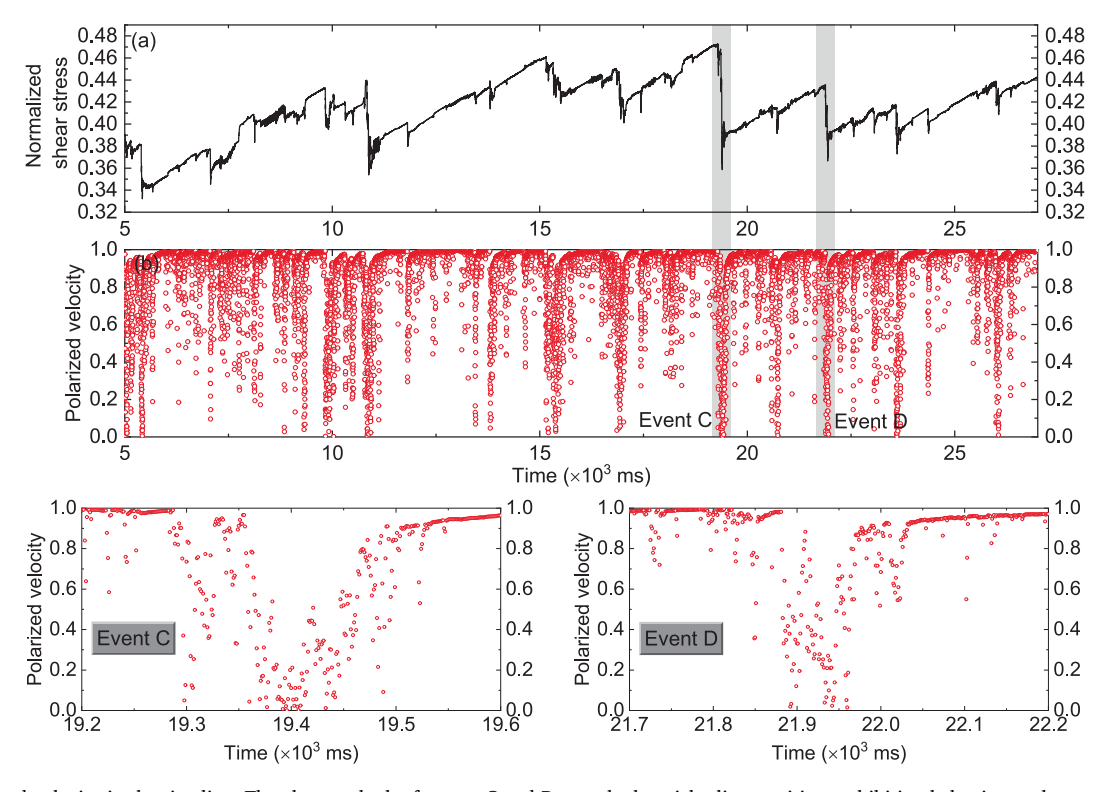


Fig. 4. Polarized velocity in the timeline. The close-up look of events C and D reveals the stick-slip transition, exhibiting behavior analogous to fluidization.

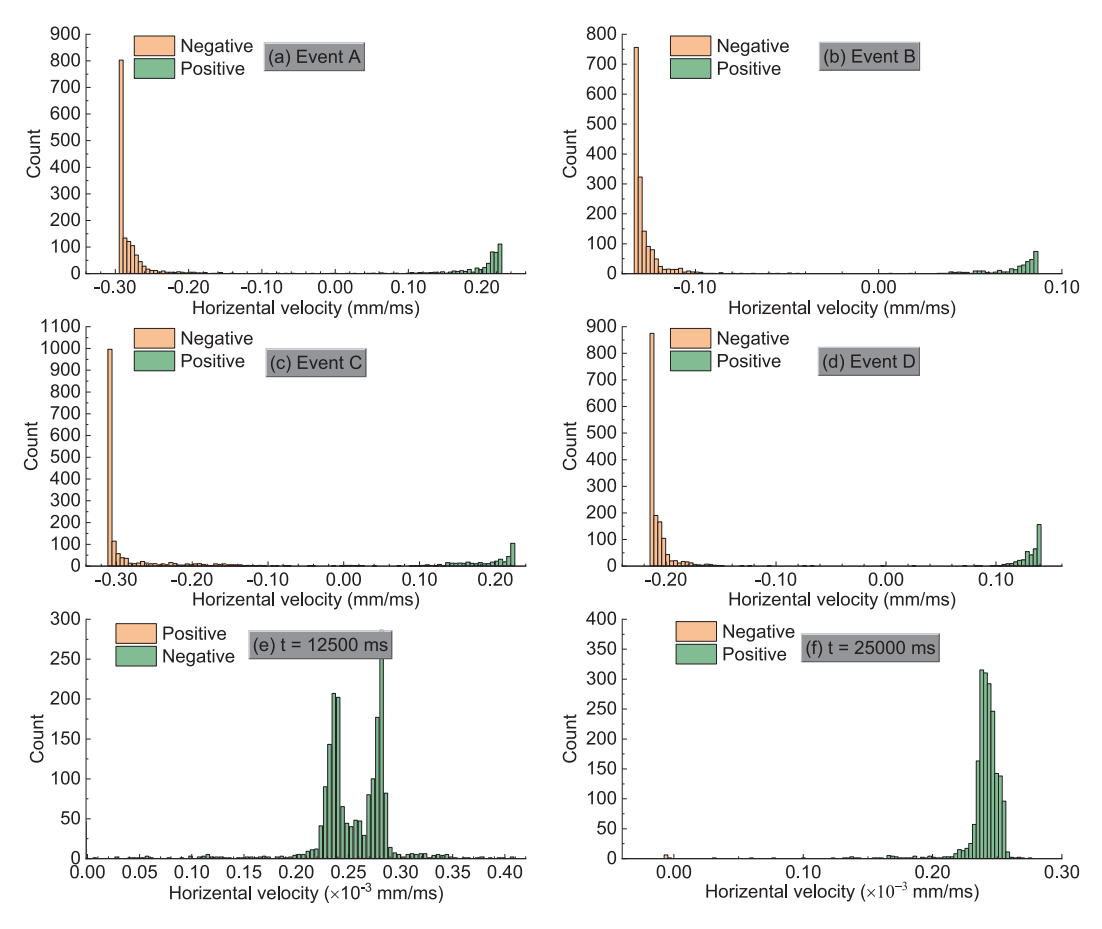


Fig. 5. Horizontal velocity, v(x), profiles of the gouge particles at (a)-(d) the four sample slip events ($Speed_{max}^A = 10,877 \text{ ms}$, $Speed_{max}^B = 16,950 \text{ ms}$, $Speed_{max}^C = 19,384 \text{ ms}$, and $Speed_{max}^D = 21,938 \text{ ms}$) and (e)-(f) two stick phases.

relative to surrounding particles, analogue to the formation of turbulent eddies in fluid flow.

3.2. Velocity correlation

The combination of large speed variance (Fig. 2c) and low polarized velocity (Fig. 4b) during fault slip explains the nature of slip events, characterized by significant particle-to-particle speed fluctuations and motion in arbitrary directions. The presence of "turbulent eddies" during fault slip suggests potential perturbations to the global correlation under shear. To further investigate particle interactions at stick–slip transition, we introduce the velocity correlation function:

$$C(d) = \frac{1}{a} \frac{\sum_{ij} u_i \bullet u_j \delta(d - d_{ij})}{\sum_{ij} \delta(d - d_{ij})}$$
 (3)

Here, the distance d is normalized by the nominally averaged particle diameter (1.4 mm, as the mean of 1.2 mm and 1.6 mm used as the gouge particle diameters); δ is the Dirac delta function; a is a normalization factor such that C(d=0)=1; u_i and u_j are the net velocities of particles i and j at a mutual distance d, which quantify the deviation of a particle's velocity from the mean:

$$u_i = v_i - \frac{1}{N} \sum_{k=1}^{N} v_k \tag{4}$$

where v_i and v_k are the velocities of particles i and k, respectively. The value of C(d) ranges from -1 to 1. Positive and negative values of C(d) respectively indicate positive and negative velocity correlations of particles at distance d, while the absolute value of C(d) reflects the strength of correlation. The analyzed gouge region comprises approximately 210 columns of particles before consolidation. Therefore, a distance d=200 is chosen as the system length, relying on the assumption that significant distortion of the gouge layer is prevented by geometrical constraints and friction under sufficiently small loads and slow shear velocity. Each particle within the gouge interacts with a finite number of neighboring particles (Goldenberg and Goldhirsch, 2002), defining the correlation within the studied spatial scale. Fig. 6 compares the velocity

correlations as a function of distance ranging from 1 to 200 particle diameters at the four sample slip events and two stick phases.

Fig. 6 clearly demonstrates two distinct regimes characterizing the two-state phase transition in the stick–slip behavior. In the stick regime, the system exhibits strong interparticle interactions, contributing to an infinite correlation length. Conversely, the slip regime is characterized by a rapid decay of velocity correlation within a spatial range of approximately eight particle diameters, beyond which the correlation fluctuates around zero. Actually, the observed decay pattern indicates significantly weakened interparticle interactions, as evidenced by the velocity correlation at d=1 being below 0.6 (see inset in Fig. 6).

In light of the distance-dependent correlation characteristics observed in the slip regime, we quantitatively examine the velocity correlations at three characteristic length scales: short-range (d=1), intermediate-range (d=10), and long-range (d=50) interactions through Eq. (3). The analysis of velocity correlation values in Fig. 6 reveals that negative correlations, ranging between -0.2 and 0, exhibit significantly weaker effects compared to their positive counterparts. To eliminate the potential bias introduced by correlation polarity, we focus our analysis on absolute values of correlation, which represent the strength of interparticle interactions regardless of their directional characteristics. Fig. 7 reports the temporal evolution of velocity correlations at these three characteristic length scales throughout the simulation, with particular emphasis on the detailed correlation patterns during events C and D.

Fig. 7 demonstrates that particles maintain strong correlations throughout the stick phase across all examined length scales. However, detailed examination of the zoomed-in views for events C and D in Fig. 7 reveals an inverse probabilistic relationship between interparticle distance and correlation strength during fault slip. The kinematic analysis indicates a synchronous variation pattern between polarized velocity (Fig. 4) and velocity correlation (Fig. 7) in response to stick–slip instabilities. This observation suggests that slip behavior is fundamentally governed system-wide correlation dynamics, which appear to be predominantly influenced by directional consistency as quantified through polarized velocity. The validity of this hypothesis and its underlying mechanisms will be systematically investigated in subsequent analyses.

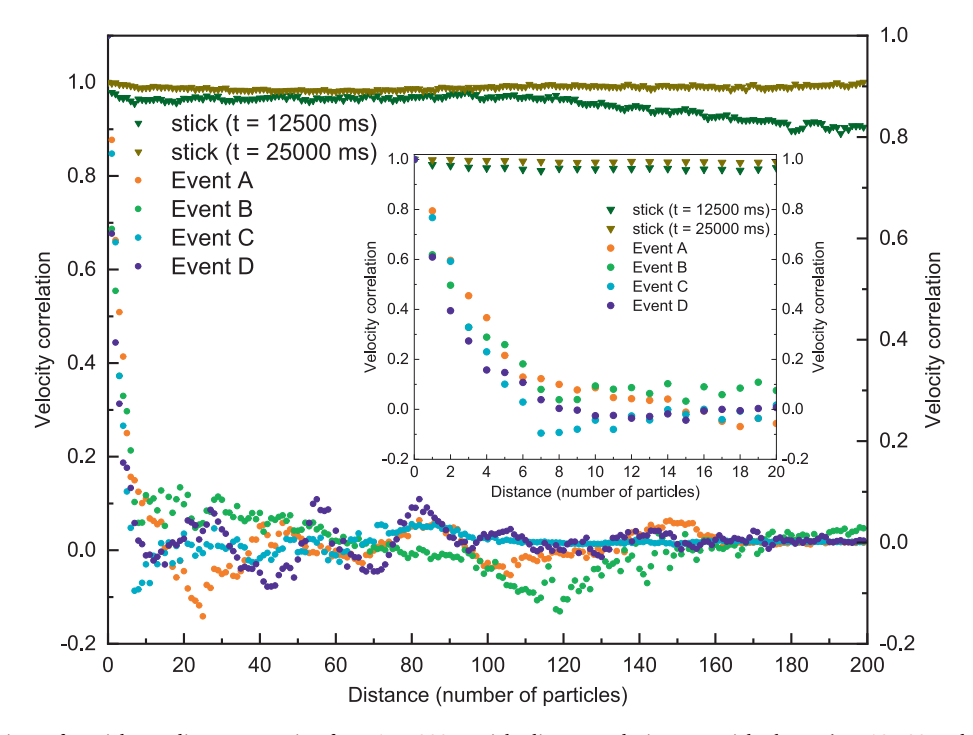


Fig. 6. Velocity correlations of particles at distances ranging from 1 to 200 particle diameters during two stick phases (t = 12,500 and t = 25,000 ms) and four sample slip events: event A (t = 10,877 ms), event B (t = 16,950 ms), event C (t = 19,384 ms), and event D (t = 21,938 ms).

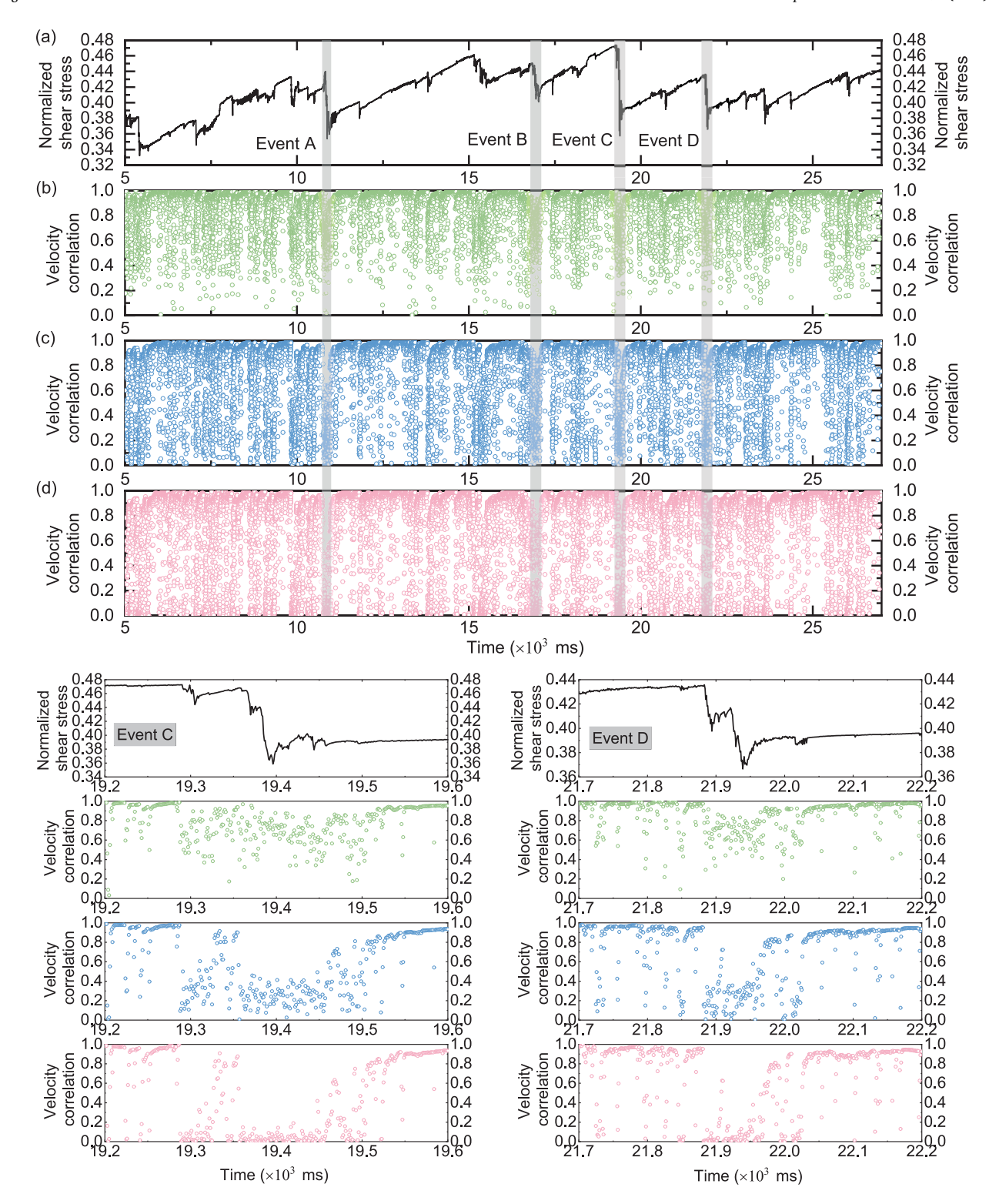


Fig. 7. (a) Temporal variation of normalized shear stress. Velocity correlations of particles at mutual distances of (b) one particle diameter (d = 1), (c) ten particle diameters (d = 10) and (d) fifty particle diameters (d = 50). The close-up look of events C and D provides a direct comparison of velocity correlations across these length scales.

3.3. Direction-dominated slip

To quantitatively characterize the relationship between polarized velocity and system correlation, we plot the scatter plot of polarized velocity versus velocity correlation in Fig. 8a. The blue dots represent average values of velocity correlation calculated at 0.02 intervals. This statistical result reveals a distinct biphasic dependency of velocity

correlation on polarized velocity, with a characteristic bifurcation point at (0.6, 0.3) (marked by the green dot in Fig. 8a). In the regime where polarized velocity remains below 0.6, velocity correlation exhibits moderate fluctuations around 0.3, demonstrating minimal dependence on directional consistency. This phenomenon reflects the breakdown of long-range correlation when particle motion becomes spatially disorganized (characterized by low polarized velocity). Conversely, within

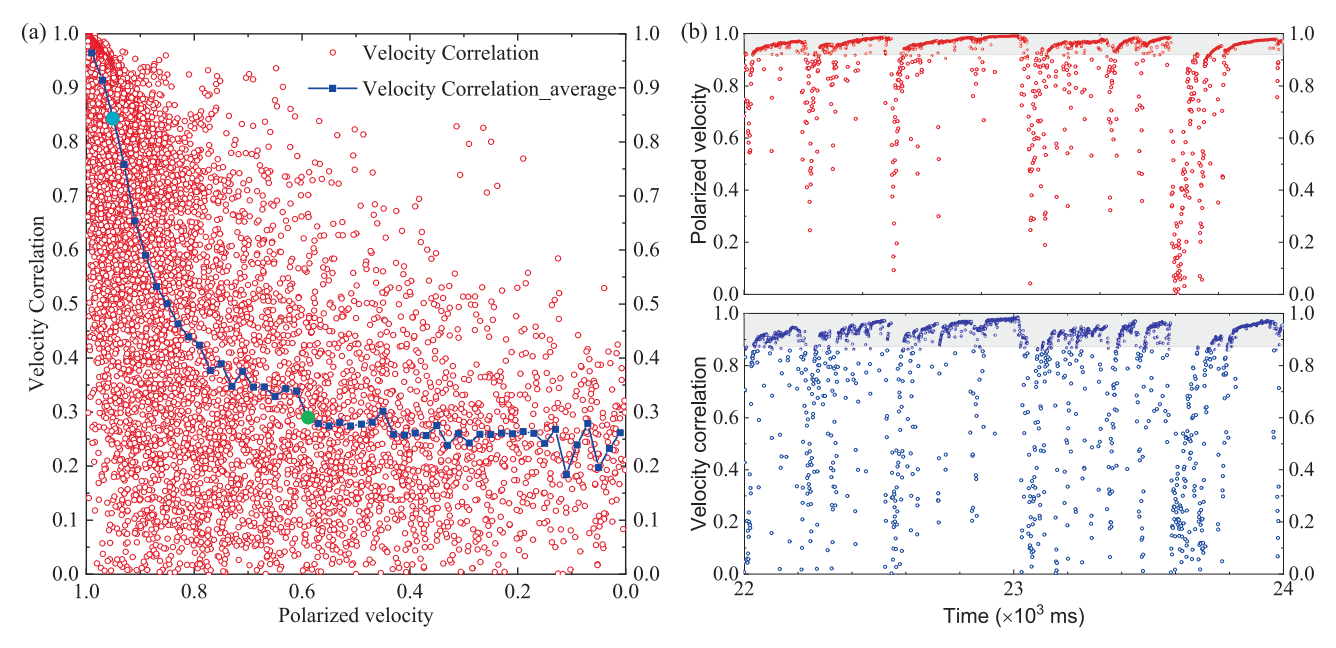


Fig. 8. (a) Scatter plot of velocity correlation versus polarized velocity. Blue dots represent the average values of velocity correlation calculated at intervals of 0.02. The cyan dot identifies the stick regime, highlighted by the shaded region in (b). The green dot marks the bifurcation point (0.6, 0.3), illustrating the dependency of velocity correlation on polarized velocity. (b) Comparison of polarized velocity and velocity correlation during the period $22-24 \times 10^3$ ms. The two shaded areas approximate the stick regime, defined by high values of polarized velocity (above 0.9) and velocity correlation (above 0.85).

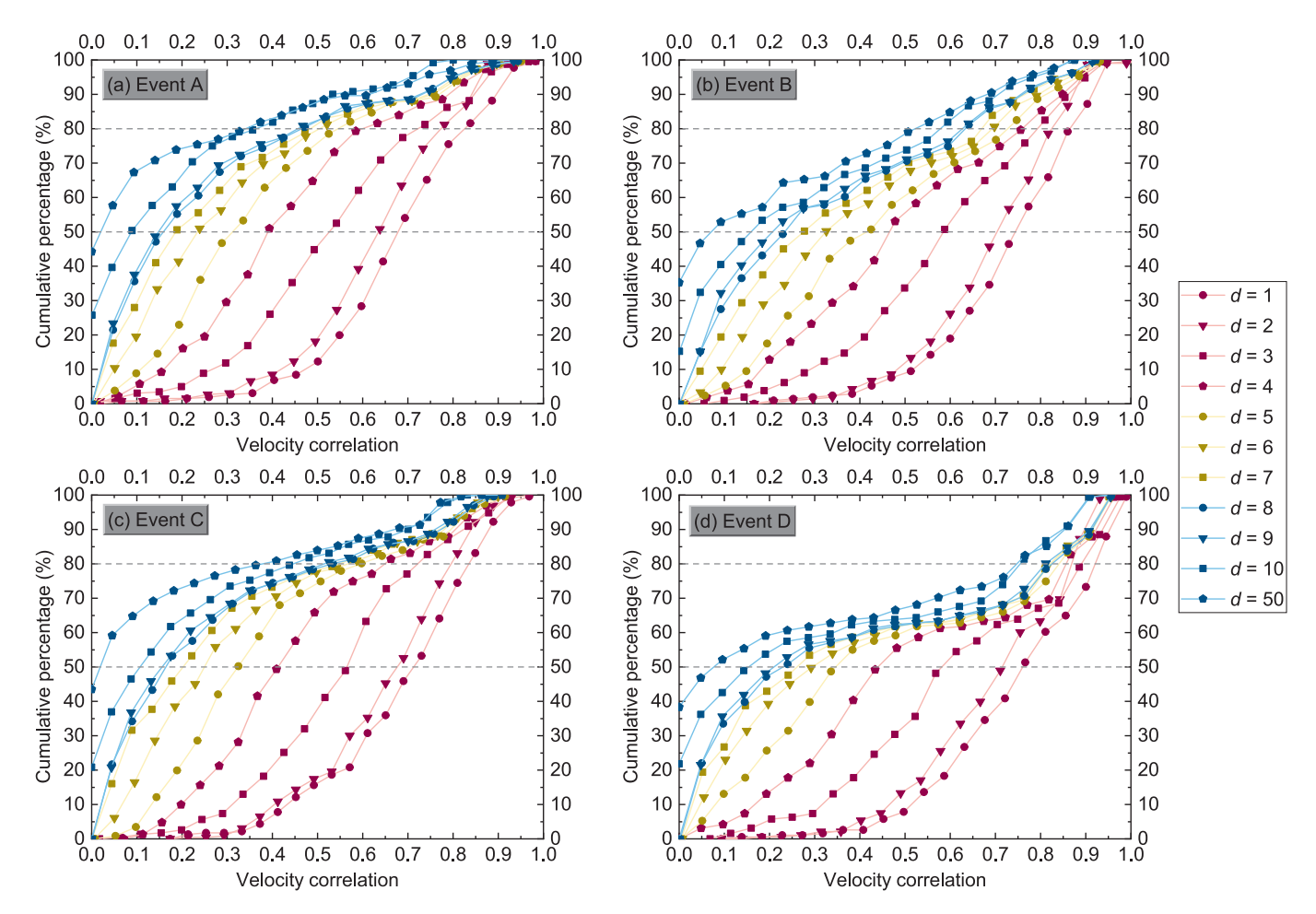


Fig. 9. The cumulative percentages of velocity correlation at various distances during events A-D (corresponding to simulation durations of 10,750 ms to 11,010 ms, 16,900 ms to 17,110 ms, 19,290 ms to 19,520 ms, and 21,840 ms to 22,030 ms, respectively). The two dashed lines respectively indicate reference thresholds of 50 % and 80 % cumulative percentages.

the polarized velocity range of [0.6, 1], a strong positive correlation emerges between velocity correlation and polarized velocity. The stick regime, however, is exclusively confined to high values of both polarized velocity (>0.9) and velocity correlation (>0.85), as indicated by the shaded region in Fig. 8b and the cyan reference dot in Fig. 8a. These findings suggest that the stick–slip transition operates in a regime where polarized velocity and system stability maintain a well-defined relationship. These results collectively indicate that the stick–slip transition is primarily attributable to the disruption of long-range correlation through the emergence of disorganized particle motion directions.

In the system under investigation, the long-range spatial correlation is established in such a way that each particle interacts with surrounding particles within a defined "interactive range". The interactive range may vary depending on a multitude of parameters, including sliding speed, normal load, surface conditions, and material combination (Berger, 2002). Within this interactive range, the spatial correlation during slip exhibits a decay with inter-particle distance, as illustrated in Fig. 7. The breakdown of long-range correlation occurs when particles lose connectivity with others within their interactive range, exciting a slip event. To quantitatively assess the interactive range in this study, Fig. 9 presents the cumulative distribution of inter-particle distances during the four slip events, providing a statistical measure of the spatial extent of particle interactions.

Fig. 9 illustrates the considerable dependence of velocity correlation on inter-particle distance during slip. With increasing distance, the slope of the cumulative percentage curve transites from an increasing to a decreasing trend. This shift from a concave to a convex curve shape indicates that stronger correlations occupy a larger percentage among particles in closer proximity. More specifically, at the 50 % benchmark, particles at a distance of one particle diameter (i.e., neighboring particles) exhibit correlations higher than 0.7, while whereas at a distance of nine particle diameters show correlations below 0.2. However, the discrepancy in correlation becomes negligible at distances exceeding eight particle diameters. This finding aligns with the observation in Fig. 6 that velocity correlation is no longer affected by distance beyond the range of approximately eight particle diameters. In other words, the interactive range in the studied system can be estimated as about eight particles, implying that the influence of distance on correlation during slip can be effectively disregarded by choosing $d \ge 8$.

4. Discussion

4.1. The solid-like to liquid-like state transition in granular materials

Granular materials like sand and foam are ubiquitous in nature and industrial applications. In the presence of external perturbations, the granular system exhibits complex mechanical behaviors resembling solids, fluids (Kou et al., 2017), gas, or intermediate phases. Theoretical studies of stick–slip phenomena indicate that the transition from stick to slip is analogous to the collapse of a solid-like state into a disordered or liquid-like state (Berman et al., 1996). Recent advances in the freezing-melting transition are generally cast in the framework of temperature differences between the two states (Makse and Kurchan, 2002; D'Anna et al., 2003). These two definitions, however, have no unified theoretical framework (Orpe and Khakhar, 2004), particularly in scenarios where solid and liquid phases coexist or metastable states are present. In such cases, neither the fluctuation–dissipation theorem adequately describes solid-like behavior nor does kinetic theory fully account for the transition criterion in fluid-like states.

Our study advances the field by systematically decoupling particle velocity magnitude and direction — a dimension seldom explored in previous research, which has predominantly focused on either velocity magnitude or force chain networks alone. By quantitatively linking the loss of directional consistency (through polarized velocity) to the collapse of system-wide velocity correlation, we provide a mechanistic, kinematics-based interpretation of the stick-slip transition. This

approach reveals that the transition is not merely an "un-jamming" event driven by kinetic energy, but rather a structural collapse of cooperative motion, where the solid-like state — defined by highly correlated, coherent particle movement — gives way to a liquid-like state characterized by localized, turbulent-like regions of disorganized motion. By bridging particle-level kinematics with collective dynamics, our framework moves beyond phenomenological analogies to establish a quantifiable, mechanism-based criterion for identifying the stick—slip transition, offering a finer-grained understanding of the micromechanisms underlying the solid-like to liquid-like transition in granular fault gouge.

4.2. Implication for prediction of natural stick-slip instability

Landslides represent a significant class of natural disasters induced by interfacial instability subject to shear deformation. Each landslide is unique in the way it develops, leading to considerable variability in both geometrical and kinematic characteristics (Angeli et al., 2000). Over the past years, various landslide monitoring systems have been developed to enhance understanding of the kinematic aspects of these disruptive processes (Carlà et al., 2019; Chang et al., 2024). In parallel, experimental (e.g. the breakdown of these long-range correlations and Zhang and Zhou, 2020; Zhou et al., 2019) and numerical (e.g., Zhang et al., 2023) methods have also been proposed, aiming to capture the precursors of such events. However, the inherent complexity emerging from the diversity of landslide types and their evolving dynamics makes monitoring data from different regions challenging to interpret and compare. This difficulty has hindered the development of theoretical models or indicators that adequately incorporate monitoring data to explain how and where a landslide failure occurs (Mondini et al., 2021). Therefore, there is a pressing need to standardize data interpretation to bridge local behaviors with the macroscopic system variables, enabling more accurate and physical-based prediction of landslide occurrence.

Given the critical yet often overlooked role of directional consistency (quantified by polarized velocity) in governing slip behavior, it is promising to develop practical indicators based on polarized velocity by integrating displacement and/or velocity field data. This study conceptualizes a framework for such an approach using displacement monitoring data (Fig. 10). To bridge the gap between numerical insight and real-world application, future work should incorporate field monitoring techniques – such as GNSS, InSAR, or ground-based radar – to validate the utility of polarized velocity as a potential indicator for landslide failure. Translating the kinematic patterns identified in this study into practical early-warning criteria would enhance our capacity for hazard prediction and risk mitigation, though their operational application requires further validation across a range of landslide scenarios.

4.3. Limitations and future work

While this study provides a detailed kinematic characterization of stick–slip behavior in a simulated fault gouge system, several limitations should be acknowledged, which also point to promising avenues for future research.

Although the analogy between stick–slip and solid–liquid transitions in granular media has been previously suggested, our study advances this concept by quantitatively decoupling the roles of velocity magnitude and direction. By explicitly linking directional disorganization to the collapse of system-wide correlation, we provide a more mechanistic basis for interpreting the transition. Future research should seek to establish a thermodynamic or statistical mechanical foundation for this behavior, particularly in systems exhibiting coexisting solid-like and fluid-like regions.

The current model is two-dimensional, which inherently simplifies the complex three-dimensional nature of real fault systems. Its geometry is based on the two-dimensional photoelastic shear experiment by Geller

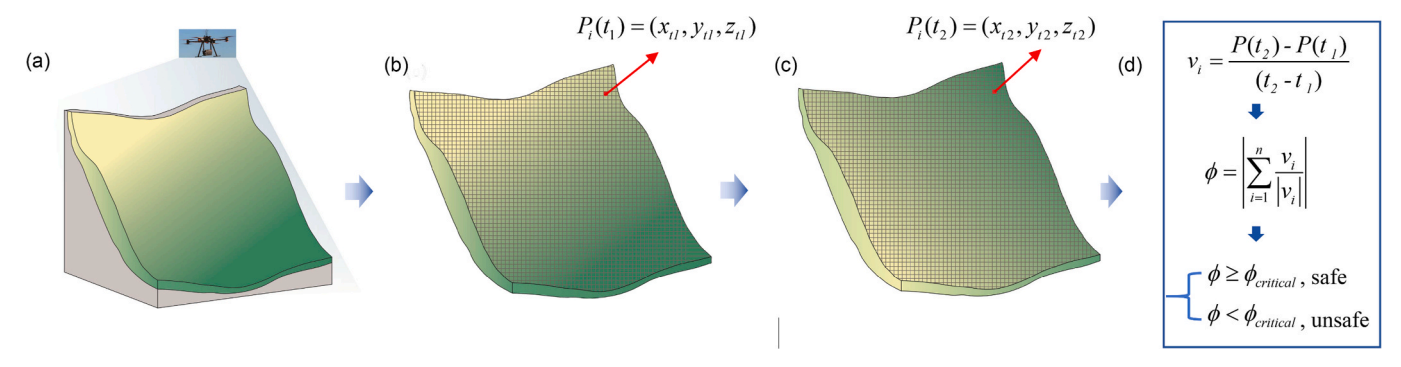


Fig. 10. Conceptual flowchart for applying polarized velocity to landslide monitoring: (a) ground surface deformation monitoring, (b) regional grid division at time t_1 with $P_i(t_1)$ denoting the position of the ith grid, (c) regional grid division at time t_2 , and (d) calculation workflow. Note that the threshold $\varphi_{critical}$ needs to be determined through extensive field calculations.

et al. (2015), and plane stress conditions are adopted for simplicity. While the model has been rigorously calibrated against these experimental benchmarks in terms of macroscopic slip behavior and stress evolution, certain dynamic properties at the particle scale (e.g., coordination number, force chain architecture, and the spatial extent of velocity correlations) are likely to differ substantially in threedimensional contexts. For instance, the constrained motion in 2D may overemphasize certain correlation patterns or inhibit the full development of turbulent-like eddies observed during slip. Nevertheless, the key qualitative behaviors identified in our simulations, such as directional disorganization and the breakdown of long-range correlation, are expected to remain relevant in 3D, albeit with quantitative differences. Although experimental determination of particle-level dynamics in 3D granular systems remains challenging, future numerical studies should extend the present framework to 3D to validate and generalize the proposed solid-like to liquid-like transition. This study thus provides a foundational and mechanistic perspective to guide future threedimensional investigations.

The system dimensions (570 mm \times 250 mm) and the analyzed region of approximately 210 particle columns raise concerns regarding potential finite-size effects. The observed velocity correlations, particularly the long-range ordering during stick phases and its rapid decay during slip, may be influenced by the limited spatial extent. In larger systems, the correlation length and the effective interactive range (identified here as approximately eight particle diameters) among particles could scale non-trivially, possibly modifying the critical dynamics of the stick–slip transition. Future studies should systematically vary the system size to assess the robustness of the observed bifurcation between polarized velocity and velocity correlation and to determine whether the proposed transition mechanism holds across scales.

5. Conclusions

In this work, we numerically develop a gouge-filled fault model to investigate the kinematic mechanisms underlying stick-slip behavior. This model interrogates interior fault details with much higher fidelity, enabling detailed examination of the mechanical performance of the deforming granular media emerging from particle-level kinematics and interactions. By isolating velocity magnitude and direction components, we quantitatively characterize the phase transition from solid-like to liquid-like state during stick-slip behavior. At the stick regime, particles exhibit coherent motion with maintained polarized velocity, generating a long-range correlated system resembling the solid-like state. As the system approaches the slip phase, particle dynamics switch into a disorganized regime marked by significant particle-to-particle speed fluctuations and localized directional variations analogue to turbulent eddies in fluid flow. These substantial perturbations disrupt the system's correlated state. This numerical framework establishes a critical connection between stick-slip motion and fault mechanics, with

particular relevance for predicting natural fault slips, such as landslides, where the data of displacement/velocity field data are accessible.

CRediT authorship contribution statement

Yahui Zhang: Writing – original draft, Validation, Funding acquisition, Formal analysis. Zifan Li: Writing – review & editing, Formal analysis. Ke Gao: Writing – review & editing, Supervision, Software, Funding acquisition. Huiming Tang: Writing – review & editing, Supervision, Funding acquisition. Changdong Li: Writing – review & editing, Supervision. Zerui Wang: Data curation.

Declaration of competing interest

The authors declare the following financial interests/personal relationships which may be considered as potential competing interests: [Yahui Zhang reports financial support was provided by National Natural Science Foundation of China (NSFC). If there are other authors, they declare that they have no known competing financial interests or personal relationships that could have appeared to influence the work reported in this paper.].

Acknowledgments

This work was supported by the Major Project of the National Natural Science Foundation of China (NSFC) (Grant No. 42090050). Acknowledgments also go to the National Natural Science Foundation of China (NSFC) (Grant No. 42307223 & 42374070).

Data availability

The data that has been used is confidential.

References

Abed Zadeh, A., Barés, J., Brzinski, T.A., Daniels, K.E., Dijksman, J., Docquier, N., Everitt, H.O., Kollmer, J.E., Lantsoght, O., Wang, D., Workamp, M., Zhao, Y., Zheng, H., 2019. Enlightening force chains: a review of photoelasticimetry in granular matter. Granul. Matter 21, 1–12.

Angeli, M.G., Pasuto, A., Silvano, S., 2000. A critical review of landslide monitoring experiences. Eng. Geol. 55 (3), 133–147.

Anthony, J.L., Marone, C., 2005. Influence of particle characteristics on granular friction. J. Geophys. Res. - Sol. Ea. 110 (B8).

Berger, E.J., 2002. Friction modeling for dynamic system simulation. Appl. Mech. Rev. 55 (6), 535–577.

Berman, A.D., Ducker, W.A., Israelachvili, J.N., 1996. Origin and characterization of different stick-slip friction mechanisms. Langmuir 12 (19), 4559–4563.

Brace, W.F., Byerlee, J.D., 1966. Stick-slip as a mechanism for earthquakes. Science 153 (3739), 990–992.

Buldum, A., Ciraci, S., 1997. Interplay between stick-slip motion and structural phase transitions in dry sliding friction. Phys. Rev. B 55 (19), 12892.

- Cao, Y., Li, J., Kou, B., Xia, C., Li, Z., Chen, R., Xie, H., Xiao, T., Kob, W., Hong, L., Zhang, J., Wang, Y., 2018. Structural and topological nature of plasticity in sheared granular materials. Nat. Commun. 9 (1), 2911.
- Carlà, T., Tofani, V., Lombardi, L., Raspini, F., Bianchini, S., Bertolo, D., Thuegaz, P., Casagli, N., 2019. Combination of GNSS, satellite InSAR, and GBInSAR remote sensing monitoring to improve the understanding of a large landslide in high alpine environment. Geomorphology 335, 62–75.
- Chang, F., Dong, S., Yin, H., Ye, X., Zhang, W., Zhu, H., 2024. Temporal stacking of subpixel offset tracking for monitoring slow-moving landslides in vegetated terrain. Landslides 21 (6), 1255–1271.
- D'Anna, G., Mayor, P., Barrat, A., Loreto, V., Nori, F., 2003. Observing brownian motion in vibration-fluidized granular matter. Nature 424 (6951), 909–912.
- Finnegan, N.J., Brodsky, E.E., Savage, H.M., Nereson, A.L., Murphy, C.R., 2022. Seasonal slow landslide displacement is accommodated by mm-scale stick-slip events. Geophys. Res. Lett. 49 (20), e2022GL099548.
- Gao, K., Euser, B.J., Rougier, E., Guyer, R.A., Lei, Z., Knight, E.E., Johnson, P.A., 2018. Modeling of stick-slip behavior in sheared granular fault gouge using the combined finite-discrete element method. Geophys. Res. - Sol. Ea. 123 (7), 5774–5792.
- Geller, D.A., Ecke, R.E., Dahmen, K.A., Backhaus, S., 2015. Stick-slip behavior in a continuum-granular experiment. Phys. Rev. E 92 (6), 060201.
- Goldenberg, C., Goldhirsch, I., 2002. Force chains, microelasticity, and macroelasticity. Phys. Rev. Lett. 89 (8), 084302.
- Gourdon, D., Israelachvili, J.N., 2003. Transitions between smooth and complex stickslip sliding of surfaces. Phys. Rev. E 68 (2), 021602.
- Hayman, N.W., Ducloué, L., Foco, K.L., Daniels, K.E., 2011. Granular controls on periodicity of stick-slip events: kinematics and force-chains in an experimental fault. Pure Appl. Geophys. 168, 2239–2257.
- Johnson, P.A., Savage, H., Knuth, M., Gomberg, J., Marone, C., 2008. Effects of acoustic waves on stick-slip in granular media and implications for earthquakes. Nature 451 (7174), 57–60.
- Kou, B., Cao, Y., Li, J., Xia, C., Li, Z., Dong, H., Zhang, A., Zhang, J., Kob, W., Wang, Y., 2017. Granular materials flow like complex fluids. Nature 551 (7680), 360–363.
- Kozlowski, R., Zheng, H., Daniels, K.E., Socolar, J.E., 2022. Stick-slip dynamics in a granular material with varying grain angularity. Front. Phys. 10, 916190.
- Lieou, C.K., Elbanna, A.E., Langer, J.S., Carlson, J.M., 2015. Stick-slip instabilities in sheared granular flow: the role of friction and acoustic vibrations. Phys. Rev. E 92 (2), 022209.

- Luan, B., Robbins, M.O., 2004. Effect of inertia and elasticity on stick-slip motion. Phys. Rev. Lett. 93 (3), 036105.
- Lyashenko, I.A., Zaskoka, A.M., 2013. Stick-slip mode of boundary friction as the first-order phase transition. arxiv preprint arxiv:1302.0720. https://doi.org/10.48550/arXiv.1302.0720.
- Makse, H.A., Kurchan, J., 2002. Testing the thermodynamic approach to granular matter with a numerical model of a decisive experiment. Nature 415 (6872), 614–617.
- Mondini, A.C., Guzzetti, F., Chang, K.T., Monserrat, O., Martha, T.R., Manconi, A., 2021. Landslide failures detection and mapping using Synthetic Aperture Radar: past, present and future. Earth Sci. Rev. 216, 103574.
- Mulliah, D., Kenny, S.D., Smith, R., 2004. Modeling of stick-slip phenomena using molecular dynamics. Phys. Rev. B 69 (20), 205407.
- Munjiza, A.A., 2004. The combined finite-discrete element method. John Wiley & Sons. Munjiza, A., Rougier, E., John, N.W.M., 2006. MR linear contact detection algorithm. Int. J. Numer. Meth. Eng. 66 (1), 46–71.
- Orpe, A.V., Khakhar, D.V., 2004. Solid-fluid transition in a granular shear flow. Phys. Rev. Lett. 93 (6), 068001.
- Pugnaloni, L.A., Carlevaro, C.M., Kozlowski, R., Zheng, H., Kondic, L., Socolar, J.E., 2022. Universal features of the stick-slip dynamics of an intruder moving through a confined granular medium. Phys. Rev. E 105 (4), L042902.
- Reddy, J.N., 2005. An introduction to the finite element method, Vol. 3. McGraw-Hill, New York.
- Shang, J., Wang, Y., Pan, D., Jin, Y., Zhang, J., 2024. The yielding of granular matter is marginally stable and critical. Proc. Natl. Acad. Sci. 121 (33), e2402843121.
- Yamada, M., Mori, J., Matsushi, Y., 2016. Possible stick-slip behavior before the Rausu landslide inferred from repeating seismic events. Geophys. Res. Lett. 43 (17), 9038–9044.
- Yoshizawa, H., McGuiggan, P., Israelachvili, J., 1993. Identification of a second dynamic state during stick-slip motion. Science 259 (5099), 1305–1308.
- Zhang, J.Z., Zhou, X.P., 2020. Forecasting catastrophic rupture in brittle rocks using precursory AE time series. J. Geophys. Res. - Sol. Ea. 125 (8), e2019JB019276.
- Zhang, Y., Gao, K., Li, C., 2023. Two slip regimes in sheared granular fault. Earth Planet. Sci. Lett. 608, 118086.
- Zheng, J., Sun, A., Wang, Y., Zhang, J., 2018. Energy fluctuations in slowly sheared granular materials. Phys. Rev. Lett. 121 (24), 248001.
- Zhou, X.P., Zhang, J.Z., Qian, Q.H., Niu, Y., 2019. Experimental investigation of progressive cracking processes in granite under uniaxial loading using digital imaging and AE techniques. J. Struct. Geol. 126, 129–145.